

## **Fluorescence and FRET based mercury (II) sensor**

Dr. Jaba Saha, Sudip Suklabaidya, Dr. Jayasree Nath, Dr. Arpan Datta Roy, Bapi Dey,

Dr. Dibyendu Dey, Prof. D. Bhattacharjee, Dr. Syed Arshad Hussain\*

Department of Physics, Tripura University, Suryamaninagar – 799022, Tripura, India

\* Corresponding author

Email: sa\_h153@hotmail.com, sahhussain@tripurauniv.in

Ph: +917005694182 (M), +91381 2375317 (O)

Fax: +913812374802

## **ABSTRACT**

A mercury (II) sensor has been proposed based on Fluorescence Resonance Energy Transfer (FRET) between N,N'-dioctadecyl thiocyanine perchlorate (NK) and Octadecyl rhodamine B chloride (RhB). Out of these two molecules NK is sensitive to  $\text{Hg}^{2+}$  ions due to presence of sulfur atom in it. Accordingly, presence of  $\text{Hg}^{2+}$  ions affects the NK fluorescence as well as FRET from NK to RhB. Our results showed that NK fluorescence intensity and FRET efficiency linearly decreases with increase in  $\text{Hg}^{2+}$  ion concentration. With proper optimization present system under investigations can be used to sense  $\text{Hg}^{2+}$  ions in aqueous solution with detection limit of 9.13 ppb. Advantage of this present system is that it is very simple compared to the other FRET based system and also it works under aqueous environment. This method has also been tested using real lake water and satisfactory results were obtained.

## **Keywords**

Fluorescence Resonance Energy Transfer

Dyes

Optical Sensor

Mercury

## **1. Introduction**

Heavy metal pollution is a serious concern in the present era as it has posed a serious threat to public health across the globe. This has made rapid detection of detrimental heavy metal ions in water as one of the most important issues because of their significant role in chemical, biological and environmental assays [1-10]. Mercury (II), one of the heavy metal ions, has been recognized as the most perilous, toxic, highly carcinogenic and hazardous pollutants; and its rampant contamination arises from a variety of natural and anthropogenic sources [11-14]. It is capable of causing serious health complications because of its close affinity to the thiol groups of enzymes and proteins. These complications may be listed as motion and central nervous system disorders, brain damage, immune system dysfunction, cardiovascular diseases, cognitive and motion disorders. It may also result in the impairment of visual and hearing senses, blindness and death for regular intake of  $\text{Hg}^{2+}$  even at a low concentration [15-20]. Mercury and its compounds have been ranked third by The United States Comprehensive Environmental Response Compensation and Liability Act (CERCLA) in the “priority list of hazardous substances” [21, 22]. Solvated mercury, which is one of the most invariable inorganic forms, is, highly toxic due to its easy water solubility [23, 24].  $\text{Hg}^{2+}$  in the contaminated natural water with its deleterious effect on human health offers the scientific community a challenging task of developing rapid, cost-effective, environmentally friendly, sensitive and selective  $\text{Hg}^{2+}$  detection methods to detect this harmful pollutant in aqueous environment. Therefore, the topic regarding detection of  $\text{Hg}^{2+}$  in aqueous environments has assumed a serious significance in the scientific mind so that its resultant health complications could be avoided [25-27].

Researchers throughout the world have shown immense interest to design  $\text{Hg}^{2+}$  sensors based on various principles. Literature survey revealed that most commonly reported methods are such as Charge Transfer (CT), Electron Transfer (ET), Energy Transfer (eT), Förster

Resonance Energy Transfer (FRET), Through bond energy Transfer (TBET), Cold Vapor Atomic Absorption Spectrometry (CVAAS), Inductively Coupled Plasma Mass Spectrometry (ICP-MS), Ultraviolet and visible spectrophotometry (UV-vis) and electrochemical methods [28-48]. Further details about various mercury detection systems have been discussed in the review paper by P. D. Selid et. al. [49].

However, fluorescence spectroscopic methods is considered as the most powerful tool for  $\text{Hg}^{2+}$  as well as other heavy metal ion detection because of its sensitivity, simplicity, inexpensive and on-site detection proficiency [41-48]. Most of the fluorescence sensors are based on either fluorescence enhancement (turn-on) or fluorescence quenching (turn off) in presence of  $\text{Hg}^{2+}$  [13-15]. These are mainly a single fluorescence signal based sensors, where, the signal may be readily disturbed by environmental perturbations e.g. pH, temperature, solvent, excitation source fluctuation, sensor concentration etc [25-27]. This can be overcome by employing ratiometric FRET based fluorescence sensing system, where, two fluorescence signals are used. Intensity of one fluorescence signal will increase and at the same time intensity of the other will decrease [1-6]. Ratio of these two signals will give idea about the sensing efficiency. As a result effect of different environmental perturbations has been eliminated automatically [50-53].

There exits few reports where, FRET phenomenon has been employed to design  $\text{Hg}^{2+}$  sensors [1-6]. However, most of these FRET based sensors work in organic/mixed solvents. Accordingly they cannot be used in most of the environmental as well as biological applications [54-56]. Therefore, it is very important to design FRET based  $\text{Hg}^{2+}$  sensing system which can work under aqueous environment [57]. Nanoparticle [36, 37] as well as quantum dot [29, 30, 35] based  $\text{Hg}^{2+}$  sensing system employing FRET are suffering from toxicity, selectivity, inadequate

resolution in aqueous environment. For most of the FRET based systems special fluorescence probes have to be designed which require rigorous and complex synthesis process [18, 53].

In the present work we report a simple FRET and fluorescence based  $\text{Hg}^{2+}$  sensing system, where two dyes NK (N,N'-dioctadecyl thiocyanine perchlorate) and RhB (Octadecyl Rhodamine B chloride) were used as FRET pair. Here, we have incorporated both the molecules onto thin film using Langmuir-Blodgett (LB) as well as Spin Coating (SC) techniques at desired mixing ratio. After that the film is dipped onto the  $\text{Hg}^{2+}$  solution (sample solution) followed by its spectroscopic analysis. Our system was capable of detecting  $\text{Hg}^{2+}$  with detection limit of 9.13 and 11.7 ppb in LB and SC film respectively.

Main advantage of the present system is that the process is very simple and no complex synthesis process is required. Also the system work under aqueous environment.

## **2. Experimental**

### *2.1. Material*

NK was purchased from Hayashibara Biochemical Laboratories Inc. RhB and mercury chloride ( $\text{HgCl}_2$ ) was obtained from Sigma Chemical Co. USA. All the salts  $\text{ZnCl}_2$ ,  $\text{FeCl}_3$ ,  $\text{AlCl}_3$ ,  $\text{MgCl}_2$ ,  $\text{CaCl}_2$ , and  $\text{CuCl}_2$  were obtained from Thermo Fisher Scientific India Pvt. Ltd. All materials were used without further purification. The dyes as well as mercury ions ( $\text{Hg}^{2+}$ ) used in our studies are positively charged. Chloroform (purity >99%, Sigma Chemical Co. USA), and ultrapure water (resistivity 18.2 M $\Omega$ ) were used as solvents.

### *2.2. SC film preparation*

The SC films were prepared by using a commercial SC Unit (SCU 2005A, APEX Instrument Co, India) operating at motor speed fixed at 6000 rpm for 60 s. In this technique

(SC), chloroform solutions of dyes are placed on a spinning solid support, followed by rotation at desired rpm.

### *2.3. Isotherm study and LB film preparation*

LB instrument (APEX-2000C, India) was used for study of monolayer characteristics and LB film deposition. Either pure water or aqueous solution of  $\text{HgCl}_2$  was used as the subphase as per requirement. Chloroform solution of NK, RhB or NK-RhB mixture was spread onto the subphase for isotherm measurement as well as for LB film deposition onto solid substrate. The concentrations of dyes used in this study were  $0.5 \times 10^{-3}$  M. LB film deposition was done at 10 mN/m surface pressure. All the experiments were done at ambient condition. Details about LB film technique have been given elsewhere [58].

### *2.4. Brewster Angle Microscopic (BAM)*

If someone interested to investigate ultrathin films on transparent dielectric substances Brewster Angle Microscopy is an ideal tool for him. When a p-polarized light incident at  $53.1^\circ$  (Brewster angle) on air-water interface, principally no reflection going to occur. So, in absence of any organic layer i.e., only in presence of water ‘black background’ will be observed. However, if a very thin layer of organic substances is present, refractive index will change. Consequently, reflection will occur. This reflected light may be utilized to obtain information about floating film. BAM instrument (Accurion nanofilm EP4-BAM, Serial No. 1601EP4030) was used for the present study. BAM images were recorded for pure NK, RhB as well as their mixture in air water interface in addition to  $\text{Hg}^{2+}$  subphase. After spreading the sample solution onto LB trough and waiting for sometimes to evaporate the solvent, images were recorded consistently at various surface pressures.

### *2.5. Spectroscopic Study*

Spectroscopic measurements (absorption and fluorescence) were carried out by Absorption Spectrophotometer (Lambda-25, Perkin Elmer) and Fluorescence Spectrophotometer (LS-55, Perkin Elmer). All the Fluorescence spectra were recorded with excitation wavelength 430 nm.

### **3. Results and discussions**

#### *3.1. FRET between NK and RhB*

Thiacyanine dye NK and xanthene dye RhB used in the present study are highly fluorescent with high quantum yield [59]. Sufficient spectral overlap exists between the fluorescence spectra of NK and absorption spectra of RhB (Figs. S1 and S2). Therefore, in principle these two dyes are suitable for FRET to occur. NK will act as donor and RhB will act as an acceptor. We have already investigated FRET phenomenon using these two dyes [59]. It has been observed that FRET occurred between these two dyes under certain conditions [59]. In homogeneous solution there was no FRET [59]. However, FRET occurred when these molecules were assembled onto restricted geometry such as clay surface as well as onto thin films [59].

Here, we have selected these two fluorophores as FRET pair to design FRET based ratiometric  $\text{Hg}^{2+}$  sensor. Pearson's Soft Hard Acid Base (SHAB) principle states that hard acids prefer to combine with hard bases and soft acids prefer to combine with soft bases resulting stable complex formation [60].  $\text{Hg}^{2+}$  ions belong to Pearson's soft Lewis acid. On the other hand, there exist two sulfur atoms in NK molecule, which belongs to soft base category. Therefore, it is expected that  $\text{Hg}^{2+}$  will form complex with NK through the interaction with its sulfur atom. This complex formation should affect the energy transfer process between NK and RhB. This is because the change in orientation as well donor-acceptor distance largely affects the extent of

FRET [61-65]. Also to best of our knowledge ratiometric  $\text{Hg}^{2+}$  sensor employing these two dyes has never been reported.

Based on our previous investigations we have planned to study FRET between NK and RhB assembled onto thin film in order to design FRET based  $\text{Hg}^{2+}$  sensor [61,66]. For ultrathin film formation LB and SC techniques have been employed.

Pure NK, RhB, and NK-RhB (50:50 molar ratio) mixture fluorescence spectra assembled onto LB films and SC films are shown in supporting information (Fig. S3). All the measurements have been performed with excitation wavelength  $\lambda_{\text{ex}}=430$  nm, which is very near to the absorption maxima of NK [59, 67]. At this wavelength, NK absorption was maximum and RhB absorption was almost negligible. This is because almost no absorption i. e direct excitation of RhB molecules occurred at this excitation wavelength (Fig. S3). However, interestingly the fluorescence spectrum of NK-RhB mixture for both the films, NK fluorescence decreases and RhB fluorescence increases in comparison to their pure counterpart. This indicates that energy transfer occurred from NK to RhB. Related fluorescence spectra are given in Fig. S3 and the spectroscopic features are listed in Table-1.

From recorded excitation spectra (inset of Fig. S3) it is affirmed that RhB fluorescence is predominantly because of the light absorption by NK and subsequent transfer it to RhB. The FRET efficiency was found to be 53% (for SC film) and 49% (for LB film) which was calculated using the following equation [59,68]

$$E = 1 - \frac{F_{DA}}{F_D};$$

Here,  $F_{DA}$  = fluorescence intensity of the donor in the presence of acceptor

$F_D$  = fluorescence intensity of the donor in the absence of the acceptor.



### 3.2. Monolayer characteristics at air water interface

In an effort to design FRET based  $\text{Hg}^{2+}$  sensor, two dyes NK and RhB has been selected as FRET pair and planned to investigate the FRET phenomenon involving these two dyes as well as  $\text{Hg}^{2+}$  assembled onto thin films. LB and SC techniques have been used for ultrathin film formation. According to Pearson's SHAB principle it is expected that  $\text{Hg}^{2+}$  will interact with NK molecules [26]. In order to have idea about the interaction between  $\text{Hg}^{2+}$  and dye molecules, here we have studied the pressure–area ( $\pi$ –A) isotherms of the monolayer of NK, RhB and NK-RhB mixture in absence (Fig. 1a) and presence (Fig. 1b) of  $\text{Hg}^{2+}$  using LB technique.

The isotherm of pure NK on water subphase started with an initial lift off area of 1.50  $\text{nm}^2$  and rises steeply until collapse pressure is reached at 59.9 mN/m. In case of pure RhB on water subphase the initial lift of area is 1.62  $\text{nm}^2$  and surface pressure rises up to 39.3 mN/m upon compression. As a whole, the shapes and the nature of  $\pi$ -A isotherms of NK and RhB are in good agreement with the previous reports [59,69,70]. However, NK–RhB isotherm has been shifted to larger area per molecule region with respect to both the pure isotherms. For the mixed isotherm the initial lift off area was 1.97  $\text{nm}^2$ . This enlargement in area per molecule for NK–RhB mixed isotherm is a clear indication about the strong interaction between the constituent molecules [71]. Due to positively charged nature of NK as well as RhB, there exists electrostatic repulsion between NK and RhB in the mixed monolayer film.

To explore the effect of  $\text{Hg}^{2+}$  on the floating monolayer, we spread NK, RhB, or NK-RhB mixture solution onto the water subphase containing  $\text{HgCl}_2$  ( $10^{-6}$  M) and recorded the corresponding isotherms. For all the case waiting time after spreading was 30 minute to allow interaction between spread molecule and  $\text{Hg}^{2+}$  in the subphase. Interestingly, NK and NK-RhB mixture isotherm in presence of  $\text{Hg}^{2+}$  showed marked change with respect to the isotherm

recorded in pure water subphase. Here, for both the isotherms area per molecules is shifted to the larger area with initial lift off area 2.01 and 2.26 nm<sup>2</sup> respectively. Area per molecule observed at 15 mN/m surface pressure was 1.23 and 1.34 nm<sup>2</sup> respectively for NK and NK-RhB mixed isotherm. On the other hand, RhB isotherm in presence of Hg<sup>2+</sup> showed almost negligible change with respect to the same measurement in water subphase. Observed change in NK and NK-RhB isotherm in presence of Hg<sup>2+</sup> indicated that there exists strong interaction between Hg<sup>2+</sup> in the subphase and the molecule (NK) onto the floating layer. As mentioned earlier, sulfur atom present in the NK molecule is a soft base and Hg<sup>2+</sup> is a soft acid. Accordingly, they will interact strongly as per SHAB rule [47]. Due to this interaction in presence of Hg<sup>2+</sup>, NK-Hg<sup>2+</sup> complex were formed at air water interface. The size of the complex is larger in comparison to that of pure NK. Accordingly, the area per molecule shifted to the larger area in case of NK and NK-RhB mixed isotherm. At the same time, for RhB, there exists almost no interaction between RhB and Hg<sup>2+</sup>. Accordingly, there was no scope for Hg<sup>2+</sup> to come onto air water interface. Consequently, area per molecule did not affect much in presence of Hg<sup>2+</sup>. Our later investigations of BAM images of floating monolayer also support this.

It has also been observed that incorporation of Hg<sup>2+</sup> onto the floating monolayer (inset of Fig. 1b) largely affected the compressibility of the floating film [72]. In presence of Hg<sup>2+</sup> compressibility of NK-RhB mixed film decreases significantly. This may be due to the fact that incorporation of Hg<sup>2+</sup> makes the floating film more rigid. Earlier reports also suggested that incorporation of metal ions enhances the rigidity of floating films [73, 74]. Therefore, lowering of compressibility of the NK-RhB mixed film prepared onto Hg<sup>2+</sup> subphase also indicated the incorporation of Hg<sup>2+</sup> onto the floating NK-RhB mixed films.

To have visual evidence about the incorporation of  $\text{Hg}^{2+}$  onto LB film we have investigated the NK, RhB and NK-RhB floating film in absence and presence of  $\text{Hg}^{2+}$  using BAM. BAM is an authentic tool generally used to get information regarding the morphological changes of the floating monolayer [66]. Accordingly, visual evidence of complex formation or interaction in the multi component LB film can be obtained through BAM studies [75].

Fig. 2 shows the BAM images recorded for NK, RhB and NK-RhB mixture LB film in presence and absence of  $\text{Hg}^{2+}$ . All the images presented here were taken at 10 mN/m surface pressure. BAM images of the same recorded at other different surface pressures are shown in Fig. S4.

From the BAM images taken at empty water surface (fig. not shown here) fully dark images has been observed. This is because; light cannot be reflected without any floating material [66]. BAM image of  $\text{Hg}^{2+}$  aqueous subphase without any dye spread onto the subphase likewise exhibited black image (fig. not shown here). Due to the water solvated nature of  $\text{Hg}^{2+}$  ions, they remained within the subphase and almost no  $\text{Hg}^{2+}$  molecules appear onto the air water interface [23, 31].

BAM images of NK and RhB on pure water subphase showed almost similar morphology (Fig. 2a and b). At the beginning at lower surface pressure the domains were smaller. Although, they were visible throughout the image and almost uniformly distributed (Figs. S4a and S4b). This corresponds to the gaseous phase of the isotherm at the beginning of the isotherm and just after the beginning of compression. With increase in surface pressure upon compression the molecules at air water interface come close to each other resulting formation of larger domains and almost compact film at the interface (Fig. 2a and b). This indicates the phase change in the floating film at higher surface pressure [70]. In case of NK-RhB mixture the surface morphology

of the floating film was different (Fig. 2c). Here the domain organization was different even at the beginning of compression i.e. very low pressure (Fig. S4c). With increase in surface pressure almost no further change was observed (Fig. 2c). Here, small islands of domains were observed throughout the image. Also, lots of blank surfaces were observed. This is because NK as well as RhB molecules were cationic and there exist repulsive interaction between these two molecules in the mixed film. Our previous isotherm studies also supported the repulsive interaction between them. Due to this repulsive interaction both NK and RhB moves away from each other. Several NK molecular domains come close to each other. Same thing happened for RhB also. As a result, colony of NK and RhB molecular domains formed throughout the film. However, it was not possible to distinguish between NK and RhB domain colony since both NK and RhB domains were almost identical (Fig. 2a and b). Also the resolution of BAM instrument did not allow this.

BAM images recorded onto  $\text{HgCl}_2$  subphase showed marked changes compared to that measured in pure water subphase (Fig. 2). In case of NK monolayer BAM images showed large domains with leaf like structures having different brightness across the domains (Fig. 2d). Even at very low surface pressure such structures were observed (Fig. S4d). As the surface pressure increases, the number of domains in addition to surface coverage increases (Fig. 2d). It has already been mentioned that according to SHAB principle  $\text{Hg}^{2+}$  interacted strongly with the floating NK and form  $\text{NK-Hg}^{2+}$  complex at air water interface [26]. Due to this interaction, domain morphology changes at the interface in presence of  $\text{HgCl}_2$  surface at the subphase [72].

At the same time, BAM images of RhB monolayer recorded in presence of  $\text{HgCl}_2$  almost identical to the same recorded in absence of  $\text{Hg}^{2+}$  (Fig. 2e). This may be due to the fact that there exists almost no interaction between the floating RhB molecule and  $\text{Hg}^{2+}$  in the subphase (Fig. S4e).

Again in case of NK-RhB mixed monolayer, presence of  $\text{HgCl}_2$  in the subphase showed marked change on the BAM images. Here, chain/wire like domains were observed throughout the image (Fig. 2f) at all the surface pressures (Fig. S4f). However at higher surface pressure the domains become more compact and several domains connect to each other. Here also the observed change may be due to the interaction of  $\text{Hg}^{2+}$  at subphase and NK in the mixed film. As a result  $\text{Hg}^{2+}$  come onto the subphase and affects the domain morphology.

Therefore, it can be concluded that BAM investigation exhibits convincing visual proof that  $\text{Hg}^{2+}$  successfully incorporated onto the NK as well as NK-RhB mixed film.

### *3.3. Fluorescence spectroscopic study of NK in thin film*

According to Pearson's SHAB rule it was expected that sulfur atom present in NK molecule will interact with the  $\text{Hg}^{2+}$  [60]. This might affect the fluorescence property of NK. Accordingly, we have prepared NK monolayer LB film and dipped the same into  $\text{HgCl}_2$  aqueous solution of different concentration ranging from  $6 \times 10^{-8}$  M to  $4.5 \times 10^{-7}$  M. After that the fluorescence spectra were recorded.

Fig. 3a showed the corresponding fluorescence spectra. Plot of fluorescence intensity (484 nm) as a function of  $\text{Hg}^{2+}$  concentrations are also plotted in the inset of Fig. 3a. Interestingly, a decrease in fluorescence intensity of NK has been found in presence of  $\text{Hg}^{2+}$ . Due to strong attraction of  $\text{Hg}^{2+}$  towards sulfur atom in NK, the lone pair on sulfur atom did not take part in resonance and hence the fluorescence intensity decreases [26]. It has been found that as the concentration of  $\text{Hg}^{2+}$  increases, fluorescence intensity of NK decreases almost linearly (inset of Fig. 3a) [76-79].

We have studied the same with SC films also. In order to do this we have prepared spin coated film of NK onto quartz substrate. The resulting film is then dipped into  $\text{HgCl}_2$  aqueous

solution of different concentration ranging from  $6 \times 10^{-8}$  M to  $4.5 \times 10^{-7}$  M followed by their fluorescence measurement. Interestingly, here also almost similar trend was observed (Fig. 3b). The fluorescence intensity almost decreases linearly with the  $\text{Hg}^{2+}$  concentrations (inset of Fig. 3b) [14].

Therefore, our fluorescence study revealed that fluorescence of NK assembled onto both LB film as well as onto SC films are highly affected by the existence of  $\text{Hg}^{2+}$  in aqueous environment. Both the cases the fluorescence intensity decreased almost linearly (inset of Fig. 3a and b) with the increase in concentration of  $\text{Hg}^{2+}$  in aqueous environment. This suggests that with proper calibration it's possible to design fluorescence based  $\text{Hg}^{2+}$  sensor using the NK LB film as well as NK SC films.

Nowadays, fluorescent sensing has turned into a robust tool for detection of different chemicals along with biological materials [41-48]. These sensors employ a single signal and records the variation in fluorescence intensity for detection, which could be easily disturbed by the environmental and instrumental perturbations [13-15]. On the other hand, FRET process involves the ratio of two fluorescence intensities at two different wavelengths simultaneously. Here, fluorescence intensity of one signal decreases and at the same time intensity decreases for the other. Idea about sensing efficiency can be obtained from the ratio [1-6]. In such manner FRET process can be a fascinating technique to design ratiometric sensors with high selectivity and simplicity [29,30, 61-65].

FRET using NK and RhB as FRET pair has already been identified [59]. Therefore, in an attempt to design FRET based ratiometric sensor for  $\text{Hg}^{2+}$  we have checked FRET process between NK and RhB in presence of various concentration of  $\text{Hg}^{2+}$ .

#### *3.4. Effect of $\text{Hg}^{2+}$ on FRET between NK and RhB in SC and LB films*

In section 3.1 of this manuscript it has been shown that FRET has taken place between NK and RhB with energy transfer efficiency 53% and 49% for SC and LB film respectively. Also it has been observed that  $\text{Hg}^{2+}$  can be successfully incorporated into LB film as well as SC films. Here to explore the effect of  $\text{Hg}^{2+}$  on FRET, we have prepared NK, RhB and NK-RhB mixed (50:50 molar ratio) SC and LB films. After that the films were dipped onto aqueous solution of  $\text{Hg}^{2+}$  at different concentrations followed by fluorescence spectroscopic measurement.

Fig. 4a and b show the plot of energy transfer efficiency vs.  $\text{Hg}^{2+}$  concentrations for LB film and SC film respectively. Related fluorescence spectra were shown in Fig. S5a and S5b. FRET parameters for both the systems were calculated using Forster theory reported elsewhere and are given in Table 2 and 3 [64]. Interestingly, it has been found that both the SC and LB films, energy transfer efficiency decreases almost linearly with increasing  $\text{Hg}^{2+}$  concentration. This gives the idea that with proper calibration it's possible to design FRET based  $\text{Hg}^{2+}$  sensor using NK and RhB as FRET pair.

### *3.5. Discussion*

Studies have shown that human health can be seriously affected due to contamination of highly toxic  $\text{Hg}^{2+}$  in drinking water [15-20]. In general mercury can exist in three different forms: elemental mercury ( $\text{Hg}^0$ ), ionic mercury ( $\text{Hg}^{2+}$ ), and organic mercury complexes [80]. Mercury can transform among these three forms based on environmental conditions [49]. Therefore, all these three forms of mercury are harmful to human health. It is important for human beings to keep away from  $\text{Hg}^{2+}$  contaminated water either to drink or everyday uses. For that reason, there is an extreme need to recognize  $\text{Hg}^{2+}$  contaminated water [1-6].

Herein, both the fluorescence intensity of NK as well as energy transfer efficiency between the fluorophores NK and RhB are found to be dependent on  $\text{Hg}^{2+}$  ion concentration in aqueous environment. Approximate linear decrease in fluorescence intensity or energy transfer efficiency was found with increasing  $\text{Hg}^{2+}$  ion concentration in aqueous environment ranging from  $6 \times 10^{-8}$  M to  $4.5 \times 10^{-7}$  M which is equivalent to 16.26 to 121.95 ppb. Therefore, it can be suggested that with proper optimization it is possible to sense  $\text{Hg}^{2+}$  in aqueous environment by observing the fluorescence intensity of NK or FRET between NK and RhB. It is already known that FRET process become a powerful tool to design various types of sensors in recent years [62,66].

Idea about the sensitivity of the proposed sensor can be obtained by calculating the Limit of Detection (LOD). It can be determined from the calibration of fluorescence as well as FRET method based on the formula  $\text{LOD} = 3\sigma/S$ , where, ' $\sigma$ ' is the standard deviation of y intercept of the regression line and ' $S$ ' is the slope of the calibration curve [24,81,82]. In the present case curve shown in Fig. 3 and 4 have been used to calculate the LOD values. The calculated values were listed in Table-4. It has been found that calculated LOD values were lower for FRET based sensing system compared to the fluorescence based sensing system. In case of fluorescence based system standard deviation of 'y intercept of the regression line' was large which resulted larger values of LOD [35, 52].

### *3.6. Selectivity of the sensor*

Practically, an effective sensor should react to a specific analyte at once; otherwise the detection procedure will have error [25]. Therefore, selectivity is a significant parameter to assess the applicability of the sensor [3-4]. In this report,  $\text{Hg}^{2+}$  levels in water can be identified by observing the decrease in fluorescence intensity or energy transfer efficiency. So, it is



extremely expected that as the concentration of  $\text{Hg}^{2+}$  changes, the energy transfer efficiency or fluorescence intensity will change with excellent selectivity.

Therefore, we examined the effect of a variety of environmentally relevant different salts on fluorescence intensity of NK as well as FRET efficiency between NK and RhB. Interestingly negligible change in fluorescence intensity (Fig. S6) and FRET efficiency (Fig. 5) occurred in presence of these salts with respect to the presence of  $\text{Hg}^{2+}$ . Values of energy transfer efficiency are given in Table 5. It has also been found that FRET based sensing system is better with respect to detection limit and sensitivity. It is interesting to mention that ratiometric fluorescence based sensors are beneficial than single fluorescence sensors because they employ the ratio of two fluorescence signals simultaneously in such a way that any fluctuations in intensity because of instrumental and environmental perturbations are cancelled out [62-65].

Fluorescence spectra's corresponding to selectivity study was shown in Fig. S6. All these observations indicate that our method described herein exhibits high selectivity and sensitivity towards  $\text{Hg}^{2+}$  in spite of the existence all possible interfering cations. This situation may be explained according to SHAB principle. According to this principle, hard acids prefer to combine with hard bases, and soft acids prefer to combine with soft bases [60]. As  $\text{Hg}^{2+}$  is a soft acid and sulfur present in NK is a soft base, the excellent selectivity towards  $\text{Hg}^{2+}$  arise due to a stronger interaction between  $\text{Hg}^{2+}$  and sulfur present in NK. Due to this attraction of  $\text{Hg}^{2+}$  towards sulfur in NK, the lone pair on S is not available for resonance and hence the fluorescence intensity of NK decreases.

On the other hand, almost no remarkable decrease in fluorescent intensity was found for other cations. Here  $\text{Cu}^{2+}$ ,  $\text{Zn}^{2+}$ , are borderline acids and  $\text{Fe}^{3+}$ ,  $\text{Al}^{3+}$ ,  $\text{Ca}^{2+}$ ,  $\text{Mg}^{2+}$  are hard acids while sulfur is a soft base. Therefore these cations do not have any affinity to come in contact

with sulfur present in NK. Therefore, there is no obvious change in the fluorescence intensity of NK in presence of these cations and also FRET remains almost unaffected.

### *3.7. Analysis of Hg<sup>2+</sup> in real water Samples.*

To demonstrate the feasibility and applicability of the planned sensing system, we have checked the proposed FRET based sensing system by using real water samples [83]. Accordingly, we have tested the proposed FRET based sensing system using natural lake water collected from three different sources. Before testing, the natural lake water was kept overnight in a beaker following filtering to remove the insoluble substances. However, no significant change in FRET efficiency was observed. This may be due to the absence of Hg<sup>2+</sup> ions in the collected water samples. As Hg<sup>2+</sup> were not found in the above real water samples, the recovery experiments were used to determine the accuracy of our method. In these experiments three different amounts of Hg<sup>2+</sup> ions were added with the collected lake water samples. After that our proposed method was applied to detect Hg<sup>2+</sup> concentrations. All the experiments were repeated three times and each result shown here is an average of three sets of independent experiments. Table -6 listed the results of recovery experiments from which it is clear that samples showed excellent recovery with (RSD) values within the range of 0.6% to 2.2% and the Hg<sup>2+</sup> recovered was within the range 95.29%-98.80% [62, 81]

## **4. Conclusion**

In summary, a simple FRET and fluorescence based Hg<sup>2+</sup> sensing system has been demonstrated by using LB as well as SC techniques. Our system was capable of detecting Hg<sup>2+</sup> with detection limit of 9.13 ppb. This method exhibits high selectivity and high sensitivity towards Hg<sup>2+</sup>. Furthermore, the system has been fruitfully used for detection of Hg<sup>2+</sup> ions in real

water with standard deviation within the range of 0.6-2.2%. Main advantage of this system is that the technique is very simple without any complex synthesis process as required for other FRET based system. Also the proposed system works under aqueous environment and can be used in most of the environmental and biological applications. Although, most of the reported FRET based  $\text{Hg}^{2+}$  sensing system work in organic/mixed solvents.

### **Acknowledgments**

The authors are grateful to DST, Govt. of India, for financial support to carry out this research work through DST project Ref: EMR/2014/ 000234 and FIST DST project Ref. SR/FST/PSI-191/2014. The authors are also grateful to UGC, Govt. of India for financial support to carry out this research work through financial assistance under UGC – SAP program 2016. The author Jaba Saha is grateful to DST-WOS-A project- Govt. of India (Ref No.: SR/WOS-A/PM-78/2016) for financial support to carry out this research work.

## References

- [1] Y. Ge, A. Liu, R. Ji, S. Shen, X. Cao, Detection of  $\text{Hg}^{2+}$  by a FRET ratiometric fluorescent probe based on a novel pyrido[1,2-a]benzimidazole-rhodamine system, *Sens. Actuator B-Chem.* 251 (2017) 410–415. doi:10.1016/j.snb.2017.05.097.
- [2] G. Singh, S.I. Reja, V. Bhalla, D. Kaur, P. Kaur, S. Arora, M. Kumar, Hexaphenylbenzene appended AIEE active FRET based fluorescent probe for selective imaging of  $\text{Hg}^{2+}$  ions in MCF-7 cell lines, *Sens. Actuator B-Chem.* 249 (2017) 311–320. doi:10.1016/j.snb.2017.04.074.
- [3] L.S. Walekar, P. Hu, H. Vafaei Molamahmood, M. Long, FRET based integrated pyrene-AgNPs system for detection of Hg (II) and pyrene dimer: Applications to environmental analysis, *Spectrochim. Acta A.* 198 (2018) 168–176. doi:10.1016/j.saa.2018.03.012.
- [4] C. Wang, D. Zhang, X. Huang, P. Ding, Z. Wang, Y. Zhao, Y. Ye, A ratiometric fluorescent chemosensor for  $\text{Hg}^{2+}$  based on FRET and its application in living cells, *Sens. Actuator B-Chem.* 198 (2014) 33–40. doi:10.1016/j.snb.2014.03.032.
- [5] P. Wang, L. Zhao, H. Shou, J. Wang, P. Zheng, K. Jia, X. Liu, Dual-emitting fluorescent chemosensor based on resonance energy transfer from poly(arylene ether nitrile) to gold nanoclusters for mercury detection, *Sens. Actuator B-Chem.* 230 (2016) 337–344. doi:10.1016/j.snb.2016.02.041.
- [6] E.S. Childress, C.A. Roberts, D.Y. Sherwood, C.L.M. LeGuyader, E.J. Harbron, Ratiometric fluorescence detection of mercury ions in water by conjugated polymer nanoparticles, *Anal. Chem.* 84 (2012) 1235–1239. doi:10.1021/ac300022y.

- [7] Q. Lin, X.-M. Jiang, X.-Q. Ma, J. Liu, H. Yao, Y.-M. Zhang, T.-B. Wei, Novel bispillar[5]arene-based AIEgen and its' application in mercury(II) detection, *Sens. Actuator B-Chem.* 272 (2018) 139–145. doi:10.1016/j.snb.2018.05.094.
- [8] P.E. Hande, A.B. Samui, P.S. Kulkarni, Selective nanomolar detection of mercury using coumarin based fluorescent Hg(II)—Ion imprinted polymer, *Sens. Actuator B-Chem.* 246 (2017) 597–605. doi:10.1016/j.snb.2017.02.125.
- [9] B. Zhang, P. Ma, D. Gao, X. Wang, Y. Sun, D. Song, X. Li, A FRET-based fluorescent probe for mercury ions in water and living cells, *Spectrochim. Acta A.*165 (2016) 99–105. doi:10.1016/j.saa.2016.04.037.
- [10] X.-C. Liang, S. Chen, J. Gao, H. Zhang, Y. Wang, J.-H. Wang, L. Feng, A versatile fluorimetric chemosensor for mercury (II) assay based on carbon nanodots, *Sens. Actuator B-Chem.* 265 (2018) 293–301. doi:10.1016/j.snb.2018.01.182.
- [11] Y. Zhang, G.M. Zeng, L. Tang, J. Chen, Y. Zhu, X.X. He, Y. He, Electrochemical sensor based on electrodeposited graphene-Au modified electrode and nanoAu carrier amplified signal strategy for attomolar mercury detection, *Anal. Chem.* 87 (2015) 989–996. doi:10.1021/ac503472p.
- [12] R. Azevedo, E. Rodriguez, Phytotoxicity of Mercury in Plants: A Review, *J. Bot.* 2012 (2012) 1–6. doi:10.1155/2012/848614.
- [13] Y. Yang, J. Jiang, G. Shen, R. Yu, An optical sensor for mercury ion based on the fluorescence quenching of tetra(p-dimethylaminophenyl)porphyrin, *Analytica Chimica Acta.* 636 (2009) 83–88. doi:10.1016/j.aca.2009.01.038.

- [14] M. Zareh Jonaghani, H. Zali-Boeini, Highly selective fluorescent and colorimetric chemosensor for detection of Hg<sup>2+</sup> ion in aqueous media, *Spectrochim. Acta A.* 178 (2017) 66–70. doi:10.1016/j.saa.2017.01.065.
- [15] K. Bera, A.K. Das, M. Nag, S. Basak, Development of a Rhodamine–Rhodanine-Based Fluorescent Mercury Sensor and Its Use to Monitor Real-Time Uptake and Distribution of Inorganic Mercury in Live Zebrafish Larvae, *Anal. Chem.* 86 (2014) 2740–2746. doi:10.1021/ac404160v.
- [16] M. Matsushita, M.M. Meijler, P. Wirsching, R.A. Lerner, K.D. Janda, A Blue Fluorescent Antibody–Cofactor Sensor for Mercury, *Org. Lett.* 7 (2005) 4943–4946. doi:10.1021/ol051919w.
- [17] Y. Zhang, Q. Yuan, T. Chen, X. Zhang, Y. Chen, W. Tan, DNA-Capped Mesoporous Silica Nanoparticles as an Ion-Responsive Release System to Determine the Presence of Mercury in Aqueous Solutions, *Anal. Chem.* 84 (2012) 1956–1962. doi:10.1021/ac202993p.
- [18] C. Ma, F. Zeng, L. Huang, S. Wu, FRET-based ratiometric detection system for mercury Ions in water with polymeric particles as scaffolds, *J. Phys. Chem. B* 115 (2011) 874–882. doi:10.1021/jp109594h.
- [19] L. Zhang, H. Chang, A. Hirata, H. Wu, Q.-K. Xue, M. Chen, Nanoporous gold based optical sensor for sub-ppt detection of mercury ions, *ACS Nano.* 7 (2013) 4595–4600. doi:10.1021/nn4013737.
- [20] Z.-X. Han, H.-Y. Luo, X.-B. Zhang, R.-M. Kong, G.-L. Shen, R.-Q. Yu, A ratiometric chemosensor for fluorescent determination of Hg<sup>2+</sup> based on a new porphyrin-quinoline dyad, *Spectrochim. Acta A.* 72 (2009) 1084–1088. doi:10.1016/j.saa.2009.01.003.

- [21] K. Chojnacka, A. Saeid, *Recent Advances in Trace Elements*, Wiley Online Books, 2018, 535.
- [22] G. Ware, *Reviews of Environmental Contamination and Toxicology*, Springer, 189 (2018) 107
- [23] J. Du, M. Liu, X. Lou, T. Zhao, Z. Wang, Y. Xue, J. Zhao, Y. Xu, Highly sensitive and selective chip-based fluorescent sensor for mercuric ion: Development and comparison of turn-on and turn-off systems, *Anal. Chem.* 84 (2012) 8060–8066. doi:10.1021/ac301954j.
- [24] N. Kaur, G. Dhaka, J. Singh, Hg<sup>2+</sup>-induced deprotonation of an anthracene-based chemosensor: set–reset flip-flop at the molecular level using Hg<sup>2+</sup> and I<sup>–</sup> ions, *New J. Chem.* 39 (2015) 6125–6129. doi:10.1039/C5NJ00683J.
- [25] A. Mohan, R. Neeroli Kizhakayil, Graphene-rhodamine nanoprobe for colorimetric and fluorimetric Hg<sup>2+</sup> ion assay, *ACS Appl. Mater. Interfaces.* 8 (2016) 14125–14132. doi:10.1021/acsami.6b03904.
- [26] K.M. Vengaiyan, C.D. Britto, K. Sekar, G. Sivaraman, S. Singaravadiel, Phenothiazine-diaminomalenonitrile based colorimetric and fluorescence “turn-off-on” sensing of Hg<sup>2+</sup> and S<sup>2–</sup>, *Sens. Actuator B-Chem.* 235 (2016) 232–240. doi:10.1016/j.snb.2016.04.180.
- [27] R.J. Maya, A. Krishna, P. Sirajunnisa, C.H. Suresh, R.L. Varma, Lower rim-modified Calix[4]arene–bentonite hybrid system as a green, reversible, and selective colorimetric sensor for Hg<sup>2+</sup> recognition, *ACS Sustain. Chem. Eng.* 5 (2017) 6969–6977. doi:10.1021/acssuschemeng.7b01158.
- [28] P. Mahato, S. Saha, P. Das, H. Agarwalla, A. Das, An overview of the recent developments on Hg<sup>2+</sup> recognition, *RSC Adv.* 4 (2014) 36140–36174. doi:10.1039/C4RA03594A.

- [29] B. Hu, L.-L. Hu, M.-L. Chen, J.-H. Wang, A FRET ratiometric fluorescence sensing system for mercury detection and intracellular colorimetric imaging in live HeLa cells, *Biosens. Bioelectron.* 49 (2013) 499–505. doi:10.1016/j.bios.2013.06.004.
- [30] S. Cui, S. Xu, H. Song, W. Xu, X. Chen, D. Zhou, Z. Yin, W. Han, Highly sensitive and selective detection of mercury ions based on up-conversion FRET from NaYF<sub>4</sub>:Yb<sup>3+</sup>/Er<sup>3+</sup> nanophosphors to CdTe quantum dots, *RSC Adv.* 5 (2015) 99099–99106. doi:10.1039/C5RA16200A.
- [31] B. Dereka, D. Svehkarev, A. Doroshenko, Facile ultrasensitive monitoring of mercury ions in water by fluorescent ratiometric detection, *Open Chem.* 11 (2013). doi:10.2478/s11532-012-0193-0.
- [32] J. Hu, L. Dai, S. Liu, Analyte-reactive amphiphilic thermoresponsive diblock copolymer micelles-based multifunctional ratiometric fluorescent chemosensors, *Macromolecules.* 44 (2011) 4699–4710. doi:10.1021/ma2001146.
- [33] N. Xia, F. Feng, C. Liu, R. Li, W. Xiang, H. Shi, L. Gao, The detection of mercury ion using DNA as sensors based on fluorescence resonance energy transfer, *Talanta.* 192 (2019) 500–507. doi:10.1016/j.talanta.2018.08.086.
- [34] D.S.-H. Chan, W.-C. Fu, M. Wang, L.-J. Liu, C.-H. Leung, D.-L. Ma, A highly selective and non-reaction based chemosensor for the detection of Hg<sup>2+</sup> ions using a luminescent Iridium(III) complex, *PLoS ONE.* 8 (2013) e60114. doi:10.1371/journal.pone.0060114.
- [35] S. Kini, V. Ganiga, S.D. Kulkarni, S. Chidangil, S.D. George, Sensitive detection of mercury using the fluorescence resonance energy transfer between CdTe/CdS quantum dots and rhodamine 6G, *J. Nanoparticle Res.* 20 (2018). doi:10.1007/s11051-018-4320-5.



- [36] B. Ma, M. Xu, F. Zeng, L. Huang, S. Wu, Micelle nanoparticles for FRET-based ratiometric sensing of mercury ions in water, biological fluids and living cells, *Nanotechnology*. 22 (2011) 065501. doi:10.1088/0957-4484/22/6/065501.
- [37] S. Pyne, G.P. Sahoo, D.K. Bhui, H. Bar, P. Sarkar, A. Maity, A. Misra, FRET based ultra sensor for detection of Hg (II) in water: A comparative study using citrate and mercapto propanoic acid as stabilizer of AuNPs, *Sens. Actuator B-Chem.* 160 (2011) 1141–1148. doi:10.1016/j.snb.2011.09.039.
- [38] A. Ono, H. Togashi, Highly selective oligonucleotide-based sensor for mercury(II) in aqueous solutions, *Angew. Chem.* 43 (2004) 4300–4302. doi:10.1002/anie.200454172.
- [39] B. Gu, Y. Bian, C.L. Miller, W. Dong, X. Jiang, L. Liang, Mercury reduction and complexation by natural organic matter in anoxic environments, *Proc. Natl. Acad. Sci.* 108 (2011) 1479–1483. doi:10.1073/pnas.1008747108.
- [40] P. Mahato, S. Saha, E. Suresh, R. Di Liddo, P.P. Parnigotto, M.T. Conconi, M.K. Kesharwani, B. Ganguly, A. Das, Ratiometric detection of Cr<sup>3+</sup> and Hg<sup>2+</sup> by a naphthalimide-rhodamine based fluorescent probe, *Inorg. Chem.* 51 (2012) 1769–1777. doi:10.1021/ic202073q.
- [41] Y. Zhao, Z. Lin, C. He, H. Wu, C. Duan, A “turn-on” fluorescent sensor for selective Hg(II) detection in aqueous media based on metal-induced dye formation, *Inorg. Chem.* 45 (2006) 10013–10015. doi:10.1021/ic061067b.
- [42] P.K. Sarkar, N. Polley, S. Chakrabarti, P. Lemmens, S.K. Pal, Nanosurface energy transfer based highly selective and ultrasensitive “turn on” fluorescence mercury sensor, *ACS Sens.* 1 (2016) 789–797. doi:10.1021/acssensors.6b00153.

- [43] T.H. Nguyen, S.P. Wren, T. Sun, K.T.V. Grattan, Fluorescent optical fibre chemosensor for the detection of mercury, in: M.R. Hutchinson, E.M. Goldys (Eds.), Adelaide, Australia, 2016: p. 100131U. doi:10.1117/12.2243054.
- [44] Z. Geng, H. Zhang, Q. Xiong, Y. Zhang, H. Zhao, G. Wang, A fluorescent chitosan hydrogel detection platform for sensitive and selective determination of trace mercury (II) in water, *J. Mater. Chem.* 3 (2015) 19455-19460. doi:10.1039/C5TA05610A.
- [45] P. Kaewanan, P. Sricharoen, N. Limchoowong, T. Sripakdee, P. Nuengmatcha, S. Chanthai, A fluorescence switching sensor based on graphene quantum dots decorated with Hg<sup>2+</sup> and hydrolyzed thioacetamide for highly Ag<sup>+</sup>-sensitive and selective detection, *RSC Adv.* 7 (2017) 48058–48067. doi:10.1039/C7RA09126E.
- [46] L. Wang, J. Tian, H. Li, Y. Zhang, X. Sun, A novel single-labeled fluorescent oligonucleotide probe for mercury(II) ion detection: Using the inherent quenching of deoxyguanosines, *J. Fluoresc.* 21 (2011) 1049–1052. doi:10.1007/s10895-010-0785-z.
- [47] X. Liu, X.-S. Zhan, F.-Y. Wu, L.-H. Ma, MnII-doped ZnS quantum dots modified with tiopronin for mercury(II) detection, *Aust. J. Chem.* (2014). doi:10.1071/CH14016.
- [48] Y.-W. Sie, C.-F. Wan, A.-T. Wu, A multifunctional Schiff base fluorescence sensor for Hg<sup>2+</sup>, Cu<sup>2+</sup> and Co<sup>2+</sup> ions, *RSC Adv.* 7 (2017) 2460–2465. doi:10.1039/C6RA24704K.
- [49] P. Selid, H. Xu, E.M. Collins, M. Striped Face-Collins, J.X. Zhao, Sensing mercury for biomedical and environmental monitoring, *Sensors.* 9 (2009) 5446–5459. doi:10.3390/s90705446.
- [50] D. Dey, J. Saha, A.D. Roy, D. Bhattacharjee, S. Sinha, P.K. Paul, S. Chakraborty, S.A. Hussain, Sensing of DNA conformation based on change in FRET efficiency between laser dyes, *Sens. Actuator B-Chem.* 204 (2014) 746–753. doi:10.1016/j.snb.2014.08.029.

- [51] N. Kumar, V. Bhalla, M. Kumar, Resonance energy transfer-based fluorescent probes for  $\text{Hg}^{2+}$ ,  $\text{Cu}^{2+}$  and  $\text{Fe}^{2+}/\text{Fe}^{3+}$  ions, *The Analyst*. 139 (2014) 543–558. doi:10.1039/C3AN01896B.
- [52] S. Wang, R. Liu, C. Li, Highly selective and sensitive detection of  $\text{Hg}^{2+}$  based on Förster resonance energy transfer between CdSe quantum dots and g-C<sub>3</sub>N<sub>4</sub> nanosheets, *Nanoscale Res. Lett.* 13 (2018). doi:10.1186/s11671-018-2647-6.
- [53] C. Ma, F. Zeng, G. Wu, S. Wu, A nanoparticle-supported fluorescence resonance energy transfer system formed via layer-by-layer approach as a ratiometric sensor for mercury ions in water, *Anal. Chim. Acta.* 734 (2012) 69–78. doi:10.1016/j.aca.2012.05.020.
- [54] H.N. Kim, M.H. Lee, H.J. Kim, J.S. Kim, J. Yoon, A new trend in rhodamine-based chemosensors: application of spirolactam ring-opening to sensing ions, *Chem. Soc. Rev.* 37 (2008) 1465. doi:10.1039/b802497a.
- [55] Y. Zhou, C.-Y. Zhu, X.-S. Gao, X.-Y. You, C. Yao,  $\text{Hg}^{2+}$ -selective ratiometric and “off-on” chemosensor based on the azadiene–pyrene derivative, *Org. Lett.* 12 (2010) 2566–2569. doi:10.1021/ol1007636.
- [56] G.-Q. Shang, X. Gao, M.-X. Chen, H. Zheng, J.-G. Xu, A novel  $\text{Hg}^{2+}$  selective ratiometric fluorescent chemodosimeter based on an intramolecular FRET mechanism, *J. Fluoresc.* 18 (2008) 1187–1192. doi:10.1007/s10895-008-0365-7.
- [57] J. Chen, A. Zheng, A. Chen, Y. Gao, C. He, X. Kai, G. Wu, Y. Chen, A functionalized gold nanoparticles and Rhodamine 6G based fluorescent sensor for high sensitive and selective detection of mercury(II) in environmental water samples, *Anal. Chim. Acta.* 599 (2007) 134–142. doi:10.1016/j.aca.2007.07.074.
- [58] A. Ulman, *An Introduction to Ultrathin Organic Films: From Langmuir–Blodgett Films of Self assemblies*, Academic Press, New York, 1991.

- [59] S.A. Hussain, R.A. Schoonheydt, Langmuir-Blodgett monolayers of cationic dyes in the presence and absence of clay mineral layers: N,N' -dioctadecyl thiocyanine, octadecyl rhodamine B and laponite, *Langmuir*. 26 (2010) 11870–11877. doi:10.1021/la101078f.
- [60] R.G. Pearson, Hard and soft acids and bases, *J. Am. Chem. Soc.* 85 (1963) 3533–3539doi: 10.1021/ja00905a001
- [61] J. Saha, A.D. Roy, D. Dey, J. Nath, D. Bhattacharjee, S.A. Hussain, Development of arsenic(v) sensor based on fluorescence resonance energy transfer, *Sens. Actuator B-Chem.* 241 (2017) 1014–1023. doi:10.1016/j.snb.2016.10.098.
- [62] D. Dey, D. Bhattacharjee, S. Chakraborty, S.A. Hussain, Development of hard water sensor using fluorescence resonance energy transfer, *Sci. Lett. J.* 184 (2013) 268-273. doi:10.1016/j.snb.2013.04.077.
- [63] J. Saha, D. Dey, A.D. Roy, D. Bhattacharjee, S.A. Hussain, Multi step FRET among three laser dyes pyrene, acriflavine and rhodamine B, *J. Lumin.* 172 (2016) 168–174. doi:10.1016/j.jlumin.2015.12.004.
- [64] J. Saha, A. Datta Roy, D. Dey, S. Chakraborty, D. Bhattacharjee, P.K. Paul, S.A. Hussain, Investigation of fluorescence resonance energy transfer between fluorescein and rhodamine 6G, *Spectrochim. Acta A.* 149 (2015) 143–149. doi:10.1016/j.saa.2015.04.027.
- [65] J. Saha, A.D. Roy, D. Dey, D. Bhattacharjee, P.K. Paul, R. Das, S.A. Hussain, Effect of zinc oxide nanoparticle on fluorescence resonance energy transfer between fluorescein and rhodamine 6G, *Spectrochim. Acta A.* 175 (2017) 110–116. doi:10.1016/j.saa.2016.12.002.
- [66] A.D. Roy, D. Dey, J. Saha, P. Debnath, D. Bhattacharjee, S.A. Hussain, Study of cholesterol derivative and phospholipid (DPPC) mixed film using LB technique and FRET:

Design of cholesterol sensor, *Sens. Actuator B-Chem.* 255 (2018) 519–528.  
doi:10.1016/j.snb.2017.08.080.

[67] D. Dey, J. Saha, A.D. Roy, D. Bhattacharjee, S.A. Hussain, Development of an ion-sensor using fluorescence resonance energy transfer, *Sens. Actuator B-Chem.* 195 (2014) 382–388. doi:10.1016/j.snb.2014.01.065.

[68] A.D. Roy, J. Saha, D. Dey, D. Bhattacharjee, S.A. Hussain, Investigation on ionic states of 1,2-Dipalmitoyl-sn-glycero-3-phosphorylcholine (DPPC) using organic laser dyes: A FRET study, *J. Lumin.* 185 (2017) 42–47. doi:10.1016/j.jlumin.2016.12.040.

[69] R.H.A. Ras, J. Németh, C.T. Johnston, E. DiMasi, I. Dékány, R.A. Schoonheydt, Hybrid Langmuir–Blodgett monolayers containing clay minerals: effect of clay concentration and surface charge density on the film formation, *Phys. Chem. Chem. Phys.* 6 (2004) 4174–4184. doi:10.1039/B405862C.

[70] D. Bhattacharjee, S.A. Hussain, S. Chakraborty, R.A. Schoonheydt, Effect of nano-clay platelets on the J-aggregation of thiocyanine dye organized in Langmuir–Blodgett films: A spectroscopic investigation, *Spectrochim. Acta A.* 77 (2010) 232–237. doi:10.1016/j.saa.2010.05.014.

[71] B. Dey, S. Chakraborty, S. Chakraborty, D. Bhattacharjee, Inamuddin, A. Khan, S.A. Hussain, Electrical switching behaviour of a metalloporphyrin in Langmuir–Blodgett film, *Org. Electron.* 55 (2018) 50–62. doi:10.1016/j.orgel.2017.12.038.

[72] M. Broniatowski, P. Dynarowicz-Łatka, Search for the molecular mechanism of mercury toxicity. Study of the mercury(II)–surfactant complex formation in Langmuir monolayers, *J. Phys. Chem. B* 113 (2009) 4275–4283. doi:10.1021/jp810339e.

- [73] S. Kundu, A. Datta, S. Hazra, Effect of metal ions on monolayer collapses, *Langmuir*. 21 (2005) 5894–5900. doi:10.1021/la0505770.
- [74] O.N.O. Jr, - Langmuir-Blodgett Films Properties and Possible Applications, *Brazilian Journal of Physics*. 22 (1992) 10.
- [75] M. Saha, A. Shil, S.A. Hussain, D. Bhattacharjee, Clay induced changes in the aggregation pattern of Safranin-O in hybrid Langmuir-Blodgett (LB) films, *J. Photochem. Photobiol. A*. 348 (2017) 199–208. doi:10.1016/j.jphotochem.2017.08.053.
- [76] Shaily, A. Kumar, N. Ahmed, Indirect approach for CN – detection: Development of “naked-eye” Hg<sup>2+</sup>-induced turn-off fluorescence and turn-on cyanide sensing by the Hg<sup>2+</sup> displacement approach, *Ind. Eng. Chem. Res.* 56 (2017) 6358–6368. doi:10.1021/acs.iecr.7b00188.
- [77] N. Wanichacheva, S. Watpathomsub, V.S. Lee, K. Grudpan, Synthesis of a Novel Fluorescent Sensor Bearing Dansyl Fluorophores for the Highly Selective Detection of Mercury (II) Ions, *Molecules*. 15 (2010) 1798–1810. doi:10.3390/molecules15031798.
- [78] E.A.K. Nivethaa, V. Narayanan, A. Stephen, Synthesis and spectral characterization of silver embedded chitosan matrix nanocomposite for the selective colorimetric sensing of toxic mercury, *Spectrochim. Acta A*. 143 (2015) 242–250. doi:10.1016/j.saa.2015.01.075.
- [79] W. Tang, Y. Wang, P. Wang, J. Di, J. Yang, Y. Wu, Synthesis of strongly fluorescent carbon quantum dots modified with polyamidoamine and a triethoxysilane as quenchable fluorescent probes for mercury(II), *Microchim. Acta*. 183 (2016) 2571–2578. doi:10.1007/s00604-016-1898-0.

- [80] T. Hou, M. Chen, G.W. Greene, R.G. Horn, Mercury Vapor Sorption and Amalgamation with a Thin Gold Film, *ACS Appl. Mater. Interfaces* 7 (2015) 23172–23181. doi:10.1021/acsami.5b07002.
- [81] M. Shyamal, S. Maity, A. Maity, R. Maity, S. Roy, A. Misra, Aggregation induced emission based “turn-off” fluorescent chemosensor for selective and swift sensing of mercury (II) ions in water, *Sens. Actuator B-Chem.* 263 (2018) 347–359. doi:10.1016/j.snb.2018.02.130.
- [82] B.K. Momidi, V. Tekuri, D.R. Trivedi, Selective detection of mercury ions using benzothiazole based colorimetric chemosensor, *Inorg. Chem. Commun.* 74 (2016) 1–5. doi:10.1016/j.inoche.2016.10.017.
- [83] G.-W. Wu, S.-B. He, H.-P. Peng, H.-H. Deng, A.-L. Liu, X.-H. Lin, X.-H. Xia, W. Chen, Citrate-capped platinum nanoparticle as a smart probe for ultrasensitive mercury sensing, *Anal. Chem.* 86 (2014) 10955–10960. doi:10.1021/ac503544w.

## Figure caption

**Fig. 1.** Pressure–area isotherm at the air–water interface (a) without  $\text{Hg}^{2+}$ , 1 = 100% RhB, 2 = 100% NK, 3 = (RhB (50%) + NK (50%)), (b) with  $\text{Hg}^{2+}$ , 1 = 100% RhB, 2 = 100% NK, 3 = (RhB (50%) + NK (50%)). Inset of Fig. 1(b) shows the Compressibility ( $C_s$ ) as a function of surface pressure for RhB (50%) + NK (50%) without  $\text{Hg}^{2+}$  (i) and with  $\text{Hg}^{2+}$  (ii) obtained from Pressure–area isotherms.

**Fig. 2.** BAM images of NK (a) RhB (b) NK-RhB (c) in water subphase and BAM images of NK (d) RhB (e) NK-RhB (f) in  $\text{HgCl}_2$  subphase. Concentrations of NK and  $\text{HgCl}_2$  are fixed at  $0.5 \times 10^{-3}$  M and  $10^{-6}$  respectively.

**Fig. 3.** Variation of fluorescence intensity of NK at different concentrations of  $\text{Hg}^{2+}$  in (a) LB films and (b) spin coating films. Concentrations of NK is fixed at  $0.5 \times 10^{-3}$  M. Concentrations of  $\text{Hg}^{2+}$  is varied from  $6 \times 10^{-8}$  M to  $4.5 \times 10^{-7}$  M. Excitation wavelength is 430 nm.

**Fig. 4.** Variation of FRET efficiency between NK and RhB at different concentrations of  $\text{Hg}^{2+}$  in (a) LB films and (b) Spin coating films. Concentrations of NK and RhB are fixed at  $0.5 \times 10^{-3}$  M. Concentrations of  $\text{Hg}^{2+}$  is varied from  $6 \times 10^{-8}$  M to  $4.5 \times 10^{-7}$  M. Excitation wavelength is 430 nm.

**Fig. 5.** FRET efficiency between NK and RhB in presence of different salts (black stacks) and in presence of different salts +  $\text{Hg}^{2+}$  (red stacks). Concentrations of NK and RhB are fixed at  $0.5 \times 10^{-3}$  M. Concentration of both  $\text{Hg}^{2+}$  and different salts are  $4.5 \times 10^{-7}$  M. Excitation wavelength is 430 nm.



Figures

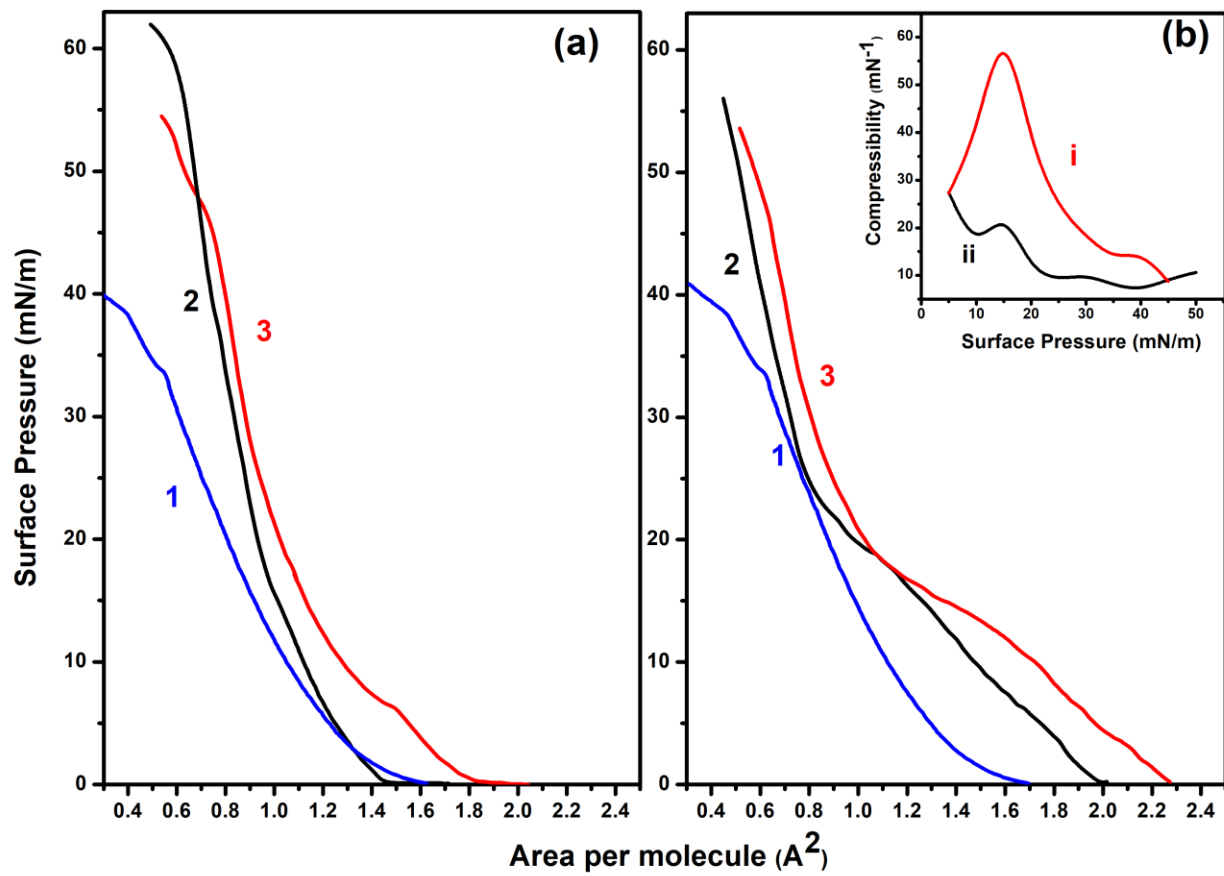
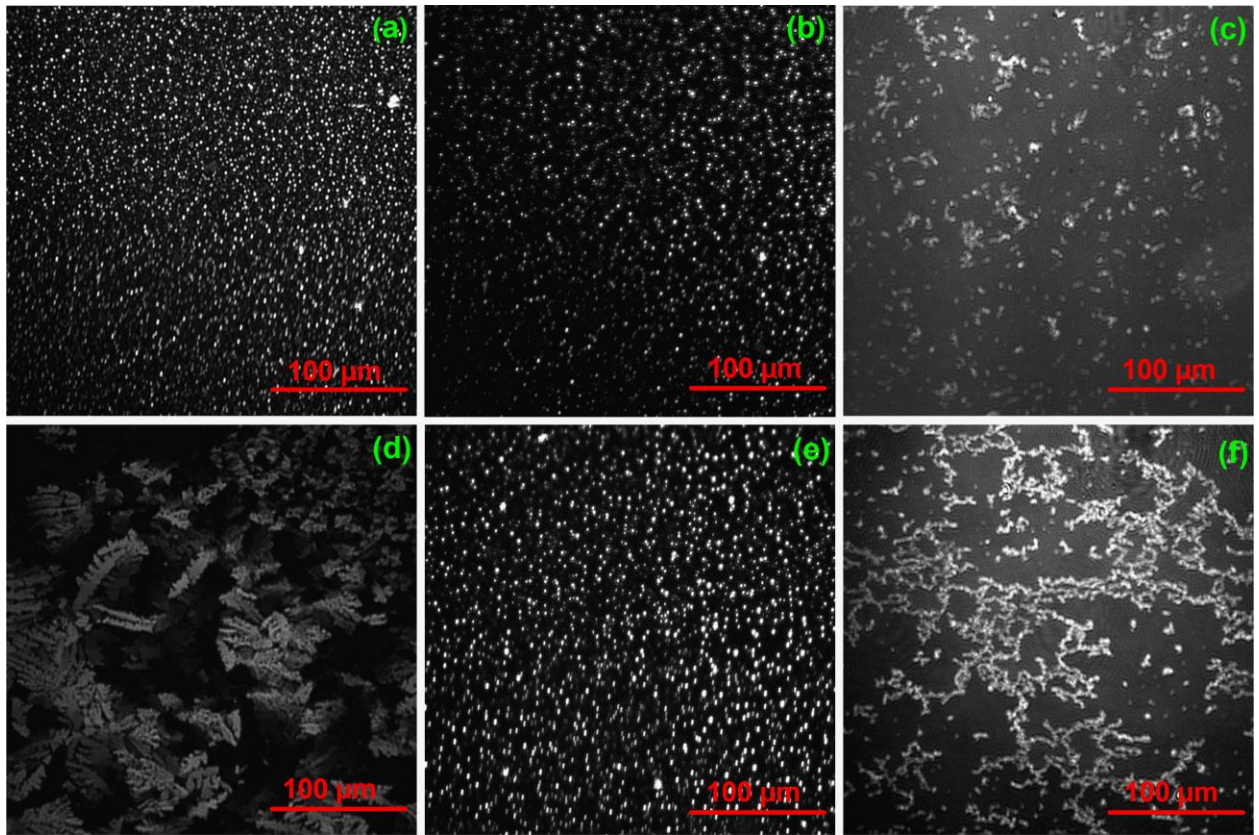


Fig. 1.



**Fig. 2.**

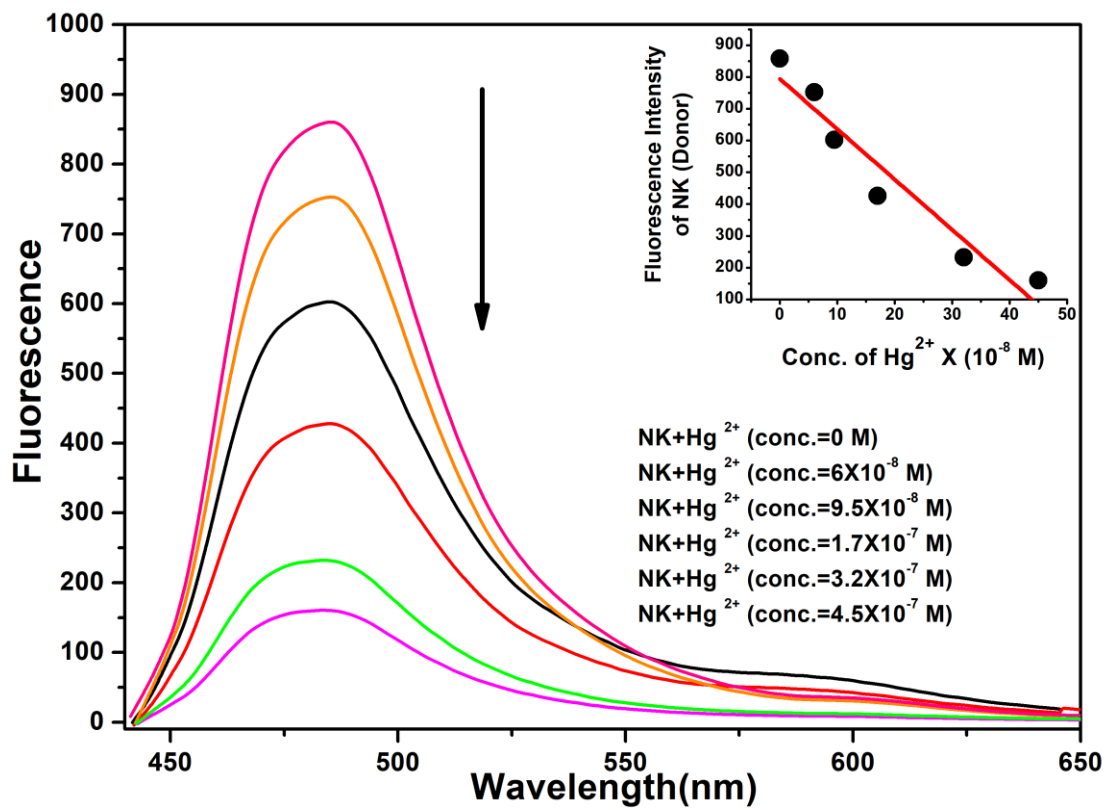


Fig. 3a.

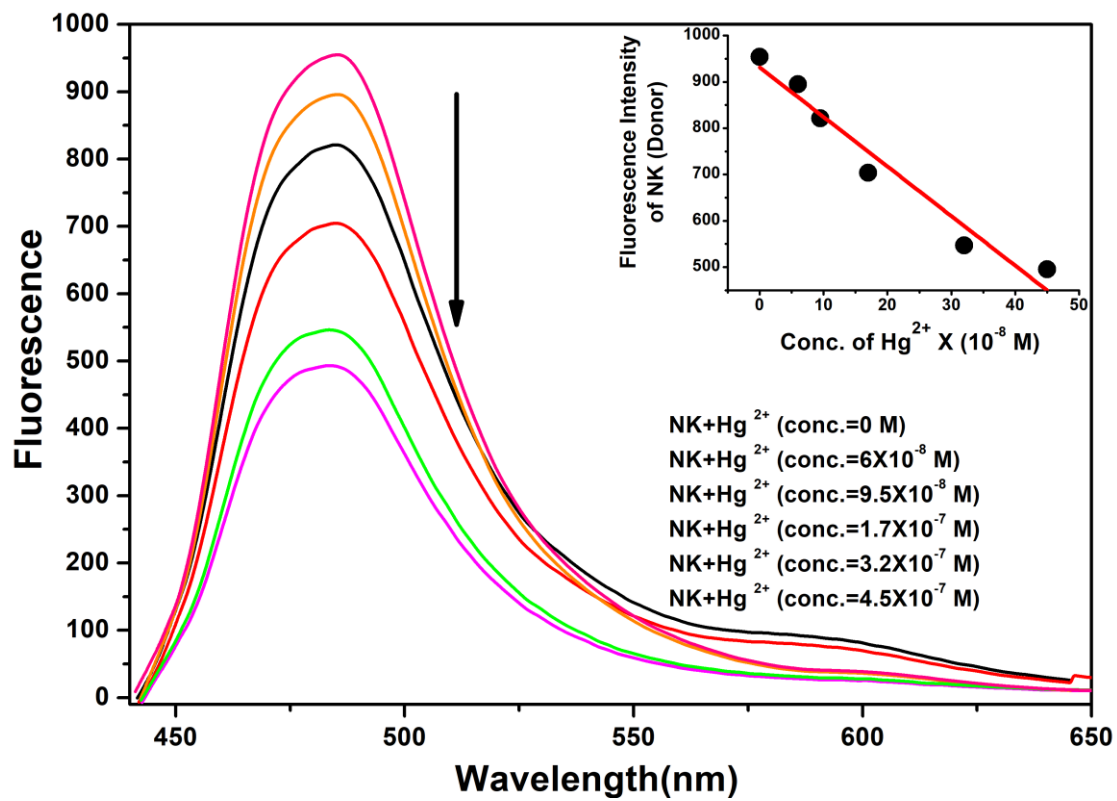


Fig. 3b.

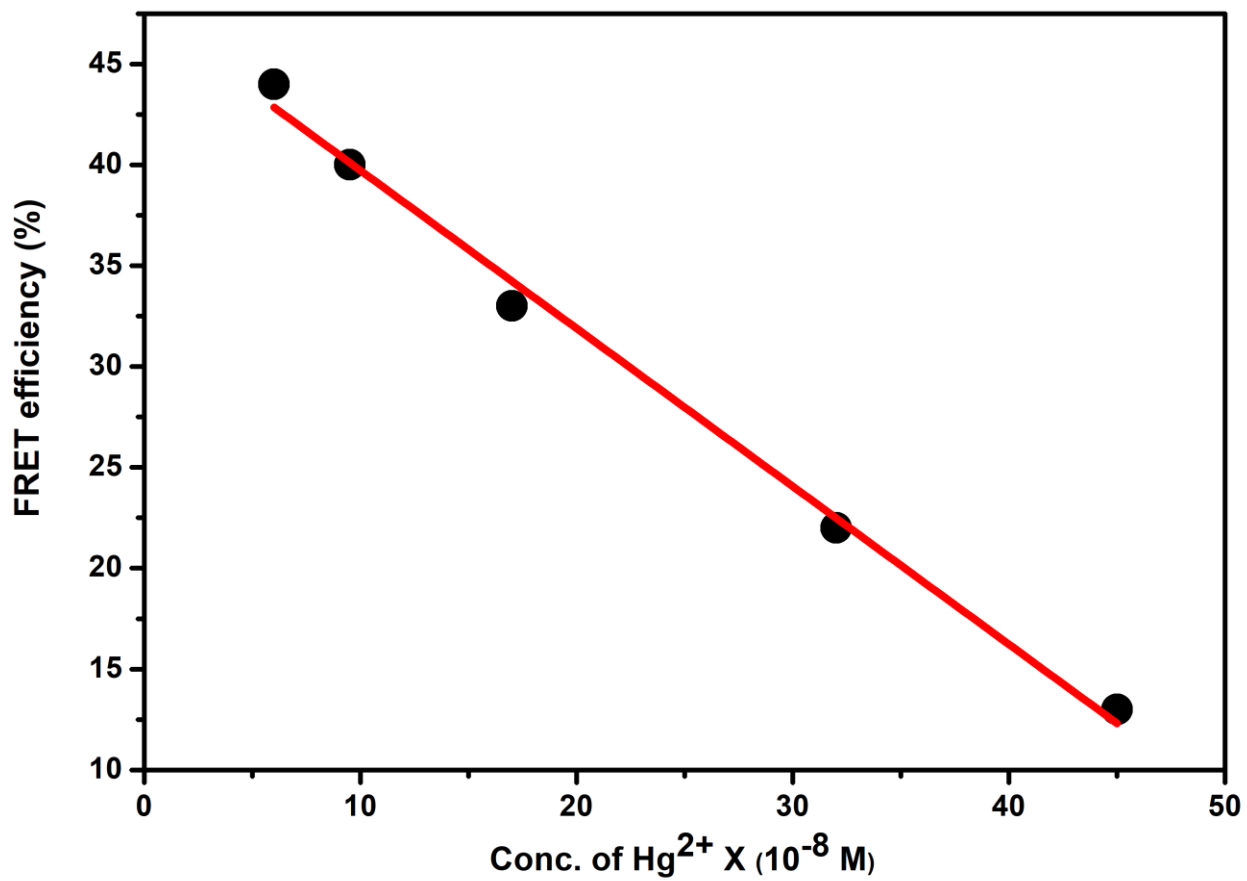


Fig. 4a.

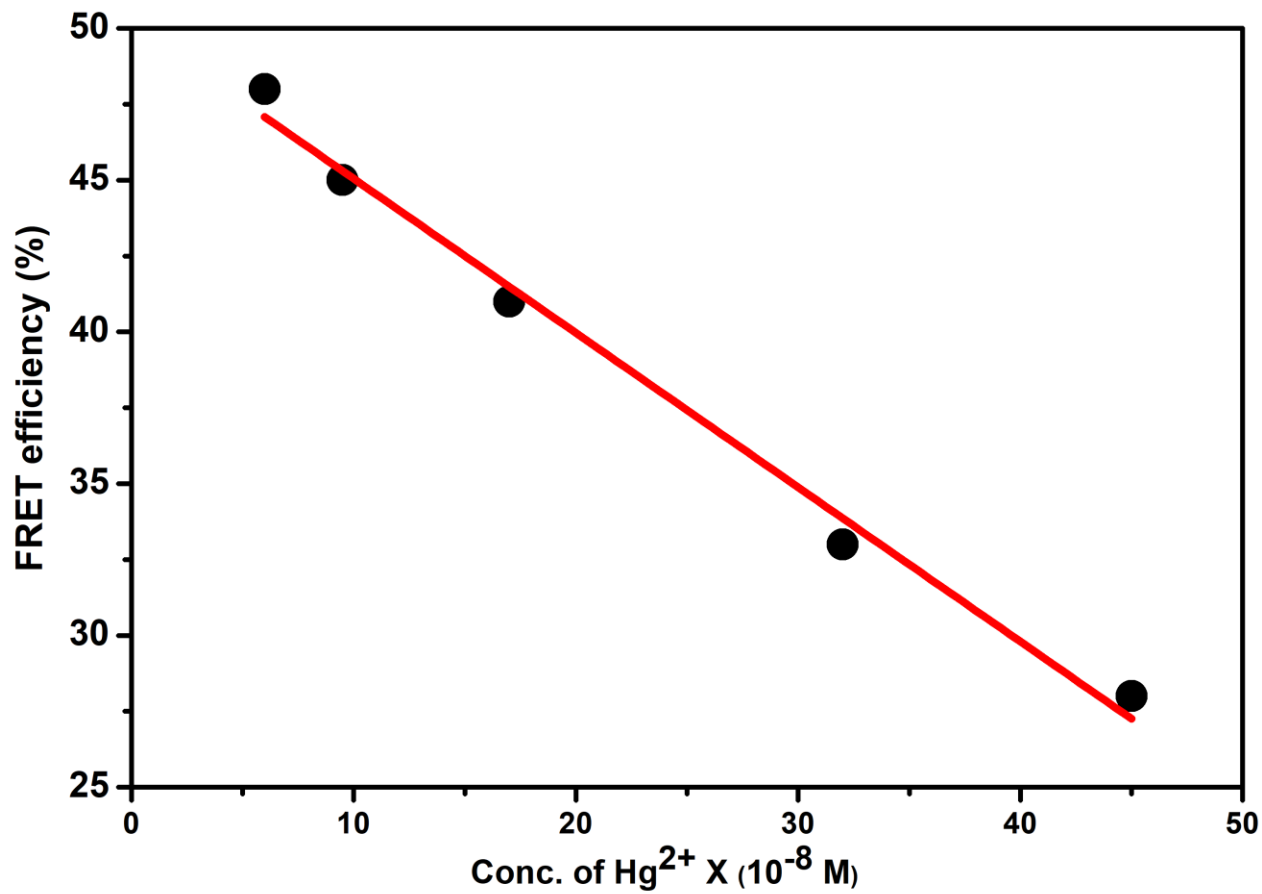


Fig. 4b.

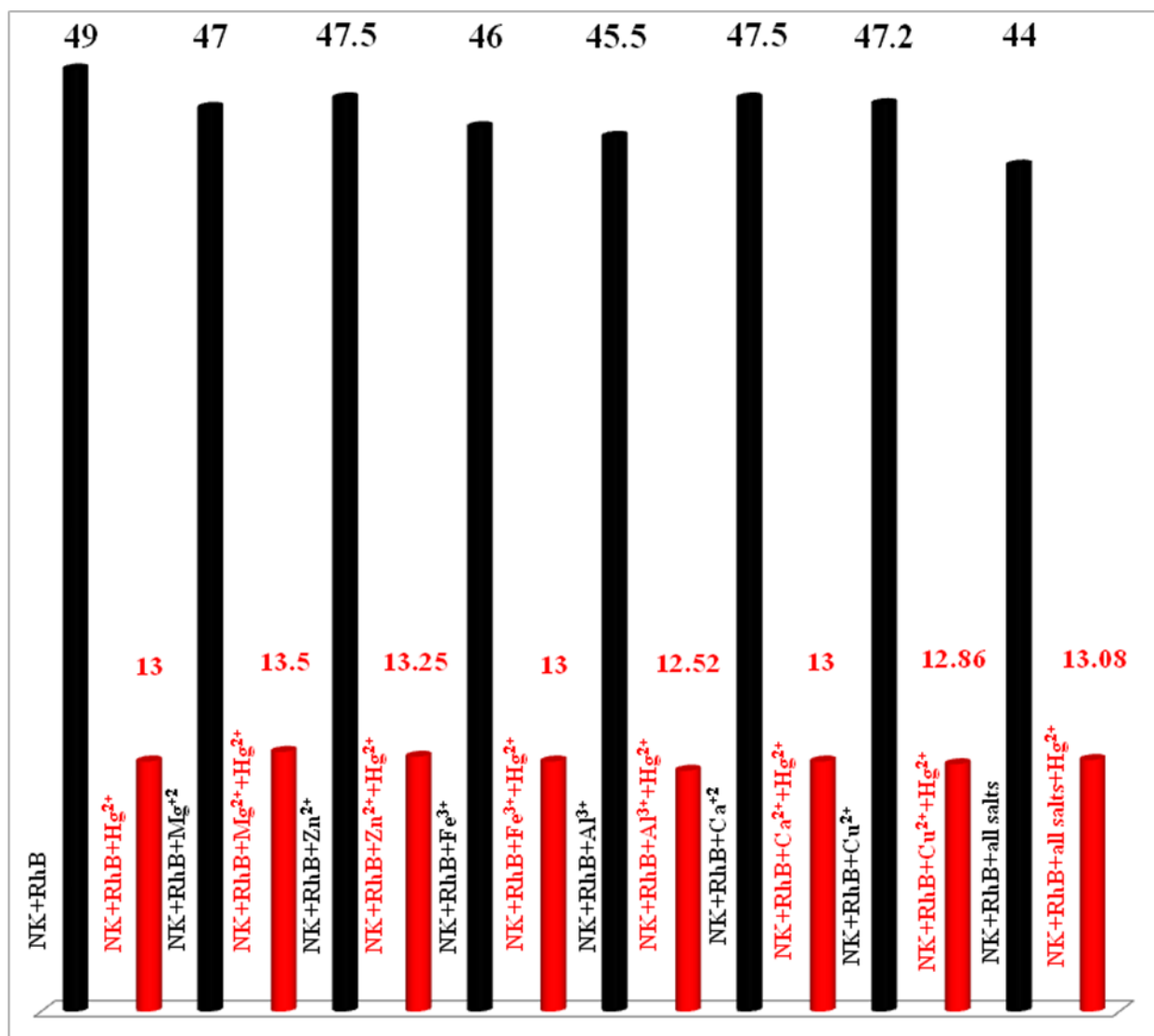


Fig. 5.

## Table caption

**Table 1.** Spectroscopic characteristics of NK and RhB in LB and SC films.

**Table 2.** Values of spectral overlap integral ( $J(\lambda)$ ), Förster radius ( $R_0$ ), donor–acceptor distance ( $r$ ) and energy transfer efficiency ( $E\%$ ) for FRET between NK and RhB with different  $Hg^{2+}$  concentration in LB films. Concentrations of both the dyes are  $0.5 \times 10^{-3}$  M. Excitation wavelength is 430 nm. These are calculated from the spectral characteristics of Fig. S3 and S5a.

**Table 3.** Values of spectral overlap integral ( $J(\lambda)$ ), Förster radius ( $R_0$ ), donor–acceptor distance ( $r$ ) and energy transfer efficiency ( $E\%$ ) for FRET between NK and RhB with different  $Hg^{2+}$  concentration in SC films. Concentrations of both the dyes are  $0.5 \times 10^{-3}$  M. Excitation wavelength is 430 nm in SC films. These are calculated from the spectral characteristics of Fig. S3 and S5b.

**Table 4.** LOD values in SC and LB films for the sensors based on fluorescence as well as FRET technique calculated from Fig. 3 and 4.

**Table 5.** Variation of FRET efficiency in presence and absence of salt and  $Hg^{2+}$ . Concentrations of NK and RhB are fixed at  $0.5 \times 10^{-3}$  M. Concentration of  $Hg^{2+}$  and different salts are  $4.5 \times 10^{-7}$  M.

**Table 6.** Determination of  $Hg^{2+}$  in sample waters.



## Tables

**Table 1**

	<b>Absorption</b>		<b>Fluorescence</b>	
	NK	RhB	NK	RhB
<b>SC film</b>	423, 442	539, 580	484	596
<b>LB film</b>	410, 433, 461	532, 573	484	600

**Table 2**

<b>Hg<sup>2+</sup> concentration (in M)</b>	<b>J(<math>\lambda</math>)<math>\times 10^{15}</math> M<sup>-1</sup>cm<sup>-1</sup>nm<sup>4</sup></b>	<b>R<sub>0</sub> (nm)</b>	<b>r (nm)</b>	<b>FRET efficiency (%)</b>
0	4.48	6.118	6.158	49
6 $\times 10^{-8}$	4.09	6.026	6.273	44
9.5 $\times 10^{-8}$	3.75	5.939	6.354	40
1.7 $\times 10^{-7}$	3.12	5.760	6.481	33
3.2 $\times 10^{-7}$	2.32	5.483	6.770	22
4.5 $\times 10^{-7}$	2.09	5.388	7.396	13

**Table 3**

<b>Hg<sup>2+</sup> concentration</b> <b>(in M)</b>	<b>J(<math>\lambda</math>)<math>\times 10^{15}</math> M<sup>-1</sup>cm<sup>-1</sup>nm<sup>4</sup></b>	<b>R<sub>0</sub> (nm)</b>	<b>r (nm)</b>	<b>FRET efficiency</b> <b>(%)</b>
0	4.80	6.189	6.066	53
6 $\times 10^{-8}$	4.50	6.123	6.205	48
9.5 $\times 10^{-8}$	4.12	6.033	6.238	45
1.7 $\times 10^{-7}$	3.99	6.001	6.376	41
3.2 $\times 10^{-7}$	3.54	5.883	6.620	33
4.5 $\times 10^{-7}$	3.21	5.788	6.774	28

**Table 4**

	<b>LB</b>		<b>SC</b>	
	<b>Adj. R<sup>2</sup></b>	<b>LOD (ppb)</b>	<b>Adj. R<sup>2</sup></b>	<b>LOD</b>
<b>Fluorescence</b>	0.886	37.64	0.927	29.53
<b>FRET</b>	0.992	09.13	0.988	11.70

**Table 5**

<b>Sample</b>	<b>Efficiency (%)</b>
(NK + RhB) + Mg <sup>2+</sup>	47.00
NK + RhB + Mg <sup>2+</sup> + Hg <sup>2+</sup>	13.50
(NK + RhB) + Zn <sup>2+</sup>	47.50
NK + RhB + Zn <sup>2+</sup> + Hg <sup>2+</sup>	13.25
(NK + RhB) + Fe <sup>+3</sup>	46.00
NK + RhB + Fe <sup>+3</sup> + Hg <sup>2+</sup>	13.00
(NK + RhB) + Al <sup>+3</sup>	45.50
NK + RhB + Al <sup>+3</sup> + Hg <sup>2+</sup>	12.52
(NK + RhB) + Ca <sup>2+</sup>	47.50
NK + RhB + Ca <sup>2+</sup> + Hg <sup>2+</sup>	13.00
(NK + RhB) + Cu <sup>2+</sup>	47.20
NK + RhB + Cu <sup>2+</sup> + Hg <sup>2+</sup>	12.86
NK + RhB + water	49.00
NK + RhB + Hg <sup>2+</sup>	13.00
(NK +RhB) + (All salts)	44.00
(NK +RhB) + Hg <sup>2+</sup> +(All salts)	13.08

**Table 6**

<b>Sample</b>	<b>Added (<math>\times 10^{-7}</math> M)</b>	<b>Found (<math>\times 10^{-7}</math> M)</b>	<b>Recovery (%)</b>	<b>RSD(% , n=3)</b>
	1.70	1.65	97.05	2.2
1#	3.20	3.10	96.80	0.6
	4.50	4.45	98.80	1.3
	1.70	1.67	98.23	0.9
2#	3.20	3.09	96.56	1.2
	4.50	4.32	96.00	1.9
	1.70	1.62	95.29	0.7
3#	3.20	3.10	96.87	2.1
	4.50	4.37	97.11	1.5